https://doi.org/10.1038/s41586-019-1447-1

Controlling organization and forces in active matter through optically defined boundaries

Tyler D. Ross[1]*, Heun Jin Lee[2], Zijie Qu[1], Rachel A. Banks[1], Rob Phillips[1,2,3] & Matt Thomson[1]*

Living systems are capable of locomotion, reconfiguration and replication. To perform these tasks, cells spatiotemporally coordinate the interactions of force-generating, 'active' molecules that create and manipulate non-equilibrium structures and force fields of up to millimetre length scales[1–3]. Experimental active-matter systems of biological or synthetic molecules are capable of spontaneously organizing into structures[4,5] and generating global flows[6–9]. However, these experimental systems lack the spatiotemporal control found in cells, limiting their utility for studying non-equilibrium phenomena and bioinspired engineering. Here we uncover non-equilibrium phenomena and principles of boundary-mediated control by optically modulating structures and fluid flow in an engineered system of active biomolecules. Our system consists of purified microtubules and light-activatable motor proteins that crosslink and organize the microtubules into distinct structures upon illumination. We develop basic operations—defined as sets of light patterns—to create, move and merge the microtubule structures. By combining these operations, we create microtubule networks that span several hundred micrometres in length and contract at speeds up to an order of magnitude higher than the speed of an individual motor protein. We manipulate these contractile networks to generate and sculpt persistent fluid flows. The principles of boundary-mediated control that we uncover may be used to study emergent cellular structures and forces and to develop programmable active-matter devices.

Our scheme is based on a well studied active system composed of stabilized microtubule filaments and kinesin motor proteins[4–8,10–12]. In the original biochemical system, kinesin motors are linked together by practically irreversible biotin–streptavidin bonds. As linked motors pull on the microtubules, a variety of phases and structures spontaneously emerge, such as asters, vortices and networks. However, spatial and temporal control of these structures is limited[5,13].

We engineered our system so that light activates reversible linking between motors (Fig. 1a) by fusing kinesin I motors to optically dimerizable iLID proteins[14]. Light patterns are projected into the sample throughout its depth and determine when and where motors link (see Supplementary Information for details). Outside the light-excitation volume the microtubules remain disordered, whereas inside the light volume they bundle and organize. The reversibility of the motor linkages allows the structures to remodel as we change the light pattern. For a cylindrical pattern of light excitation, the microtubules contract into a three-dimensional aster (Fig. 1b, Supplementary Information section 2.1, Supplementary Videos 1, 2). We use the projection of a cylinder of light as an operation for creating asters. We note that vortices, spirals, and extensile behaviour are not observed under our conditions (Supplementary Information section 2.2).

Our temporal control over aster formation allows us to study the dynamics of their creation and decay (Fig. 1c, Supplementary Video 3) through time-lapse imaging (Supplementary Information section 2.3). We characterize these dynamics by measuring the spatial width of the distribution of fluorescently labelled microtubules using the image standard deviation (Supplementary Information section 2.4). During aster formation, the distribution of microtubules within a cylinder pattern contracts. After 10–15 min, the distribution reaches a steady state, indicating that the aster is fully formed. To quantify the characteristic aster size (Supplementary Information section 2.5), we measure the image standard deviation at 15 min (Supplementary Information section 2.6). Once the excitation light is removed, the asters begin to decay into free microtubules. The spatial distribution of the microtubules widens over time, returning to the initial uniform distribution. Further, the aster decay is reversible (Supplementary Information section 2.7).

To understand the scaling behaviour of the system, we investigate how the dynamics of aster formation and decay depend on the excitation volume. During formation, microtubule distributions contract. The contraction speed (Supplementary Information section 2.8) grows with the diameter of the excitation cylinder (Fig. 1d). Similar scaling of the contraction speed has been observed for actomyosin systems[15] (Supplementary Information section 2.9) and modelled for generic networks[16]. Alternatively, contraction can be quantified by a characteristic contraction timescale[17] (see Supplementary Information section 2.8). During decay, microtubule distributions spread in a manner consistent with diffusion (Supplementary Information section 2.10). The effective diffusion coefficient is independent of the characteristic aster size (Fig. 1e) and is consistent with what is expected for free microtubules (Supplementary Information section 2.11). Further, we manipulate the aster size through the diameter of the excitation volume (Fig. 1f) and find a scaling dependence (Supplementary Information section 2.12) that shows similarities to the dependence of spindle size on confining volumes[18].

Moving activation patterns are responsible for dynamically repositioning structures and forces within a cell[19]. Similarly, we can move asters by repositioning the light patterns relative to the sample slide by moving the slide stage (Fig. 2a). We are also able to move asters by directly moving the light pattern; however, moving the stage allows a greater range of travel. As the stage moves, the asters track the light pattern, travelling up to hundreds of micrometres relative to the slide (Fig. 2b, Supplementary Video 4, Supplementary Information section 2.13). The aster maintains a steady-state distance ℓ between itself and the light pattern (Fig. 2c). We find that the asters are able to track the pattern for stage speeds of up to 200 nm s^{-1}. At 400 nm s^{-1} the asters cannot stay with the pattern, resulting in an 'escape velocity' that is comparable to the motor speeds measured in gliding assays (Supplementary Information section 2.16). When the stage stops moving, the aster returns to the centre of the light pattern, indicating that the aster is experiencing a restoring force. We can characterize the aster movement caused by an effective potential (Supplementary Information section 2.14) and observe mesoscopic phenomena that may clarify the underlying mechanisms of the aster motion (Supplementary Information section 2.15).

Intriguingly, we find that asters formed near each other interact by spontaneously merging. To study this interaction, we construct an aster merger operation, where asters are connected with light (Fig. 2d,

---

[1]Division of Biology and Biological Engineering, California Institute of Technology, Pasadena, CA, USA. [2]Department of Applied Physics, California Institute of Technology, Pasadena, CA, USA. [3]Department of Physics, California Institute of Technology, Pasadena, CA, USA. *e-mail: tross@caltech.edu; mthomson@caltech.edu

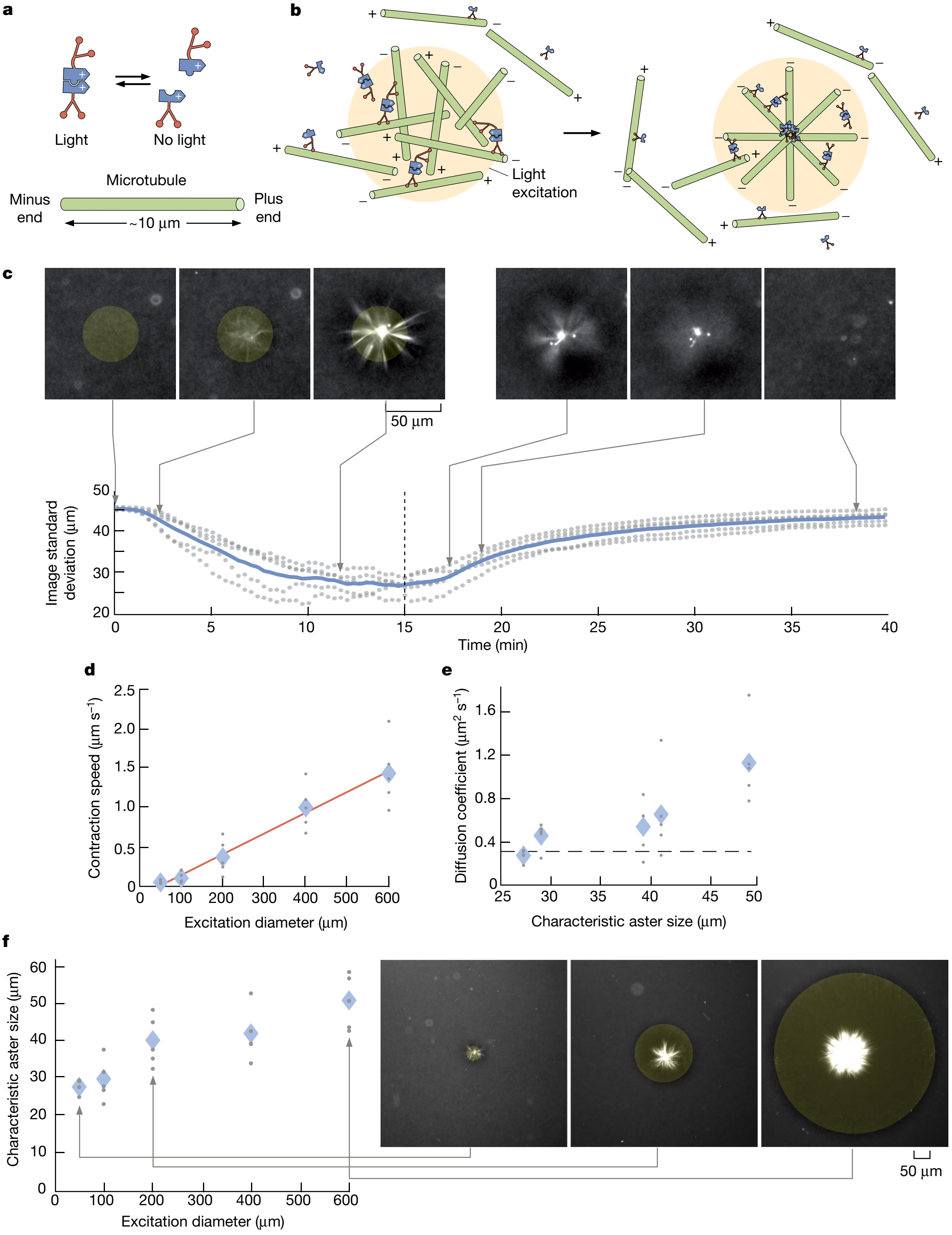

Fig. 1 | The light-switchable active-matter system enables optical control over aster formation, decay and size. **a**, Schematic of light-dimerizable motors that walk towards the plus ends of stabilized microtubules. **b**, Schematic of light-controlled reorganization of microtubules into an aster, where locally dimerized motors pull microtubule plus ends towards each other. **c**, Images of labelled microtubules during aster assembly and decay (top), and corresponding plots of the image spatial standard deviation versus time (bottom). The blue line is the mean of five experiments and the grey dots represent individual experiments. The dashed line shows the time at which the activation light is removed, indicating the transition from creation to decay. **d**, Maximum contraction speed versus excitation diameter. The red line is a linear fit. **e**, Diffusion coefficient versus characteristic aster size. The characteristic size is the image spatial standard deviation at the 15-min time point shown in **c**. The dashed line represents the diffusion coefficient of a 7-µm-long microtubule (Supplementary Information section 2.11). **f**, Characteristic aster size versus excitation diameter (left) and representative images (right). In **d**–**f** the blue diamonds represent the mean of five experiments and the grey dots represent individual experiments. In **c**, **f** the yellow-shaded disks represent the light pattern.

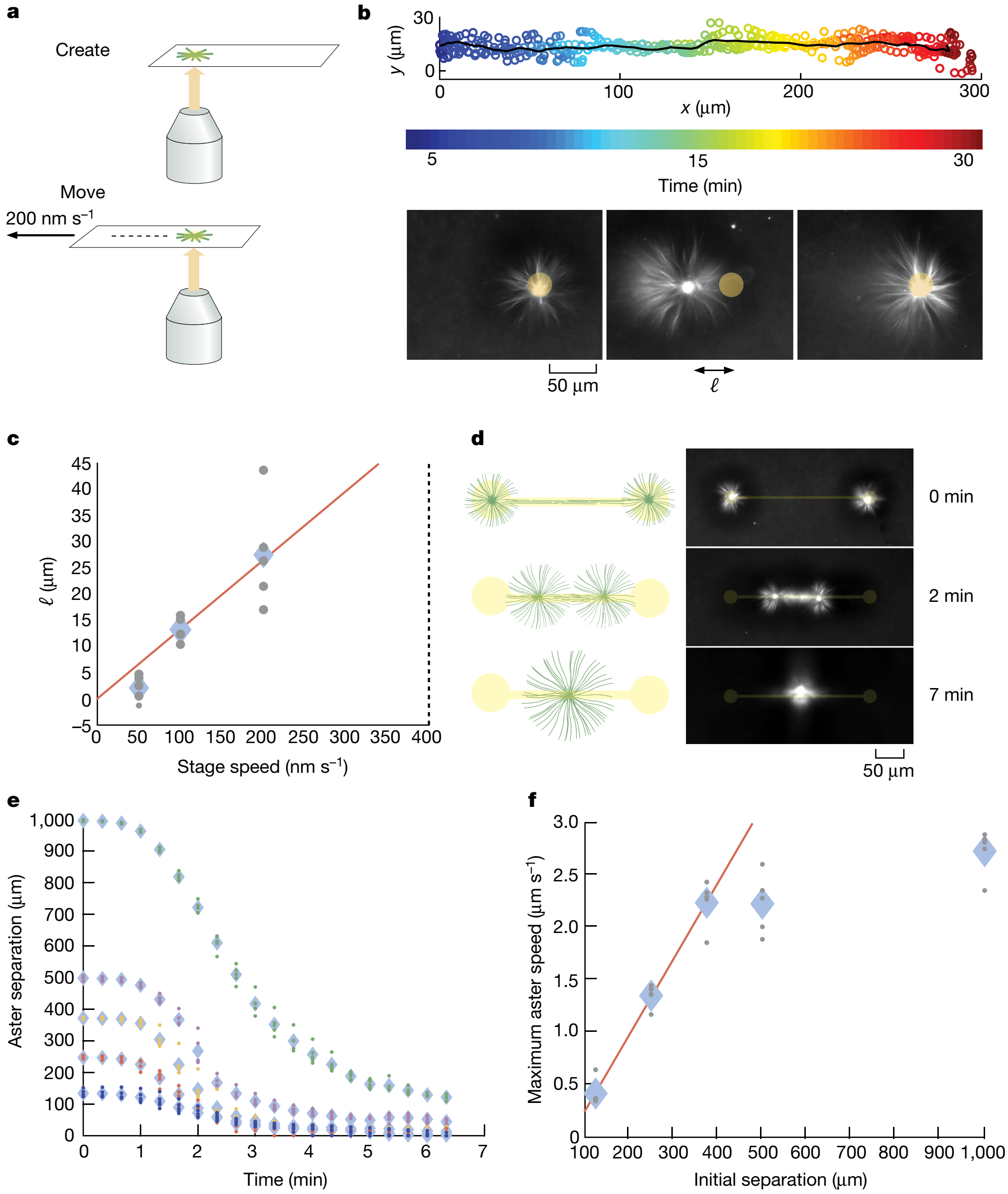

Fig. 2 | Moving and merging operations of asters with dynamic light patterns. a, Asters are moved relative to the slide by repositioning the microscope stage. **b**, Overlay of five individual trajectories of aster movement relative to the slide, which is moving at 200 nm s^{-1} (top). The black line represents the mean trajectory. The time-lapse images show the position of the aster relative to the light pattern. ℓ is the displacement of the aster from the centre of the light pattern. **c**, ℓ versus stage speed. The dotted line at 400 nm s^{-1} represents the escape velocity. The red line is a linear fit. **d**, Illustration of the aster merging operation by a connected excitation pattern (left) and the corresponding time series of images (right). **e**, Distance between merging asters over time for different initial separations. **f**, Maximum speed of asters, as measured from **e**. The red line is a linear fit to the first three data points. In **c**–**f** the blue diamonds represent the mean of five experiments and the dots represent individual experiments.

Supplementary Video 5). At the beginning of the merging process, a network of bundled microtubules forms, which connects the asters. The connecting network begins to contract and the asters move towards each other (Fig. 2e). The speed at which asters merge (Supplementary Information section 2.8) increases as a function of linking distance up to a speed of roughly 2.5 µm s^{-1} (Fig. 2f). The scaling of the aster merger speed as a function of distance is similar to the observed relationship of the contraction speed with the excitation cylinder size discussed above. We note that the maximum observed merger speed is about an order of magnitude higher than the speeds observed during gliding assays (Supplementary Information section 2.16), which is analogous to how cell-migration speeds can exceed single-motor speeds[20]. Our ability to move and merge microtubule asters reveals that they are not steady-state structures, as previously reported[5], but that they are dynamic and constantly remodelling.

Having the capability to perform successive operations remains a fundamental step towards engineering with active matter. Our ability to form dynamic light-defined compartments of active molecules enables us to execute multiple aster operations. By combining aster creation operations, we can form asters of differing sizes and place them at prescribed positions in parallel (Fig. 3a, b, Supplementary Video 6). Once asters are created, they can be simultaneously moved using multiple dynamic light patterns (Fig. 3c, d, Supplementary Video 7). Further, the aster trajectories are not limited to rectilinear motion but can be moved along complex trajectories (Fig. 3e, f, Supplementary Video 8). During movement, there are inflows of microtubule bundles created in the light pattern, which feed into the aster. There are also outflows of microtubules, which appear as comet-tail streams following the asters (Fig. 3d, f). These mass flows illustrate some of the complex non-equilibrium dynamics that are introduced by moving boundaries

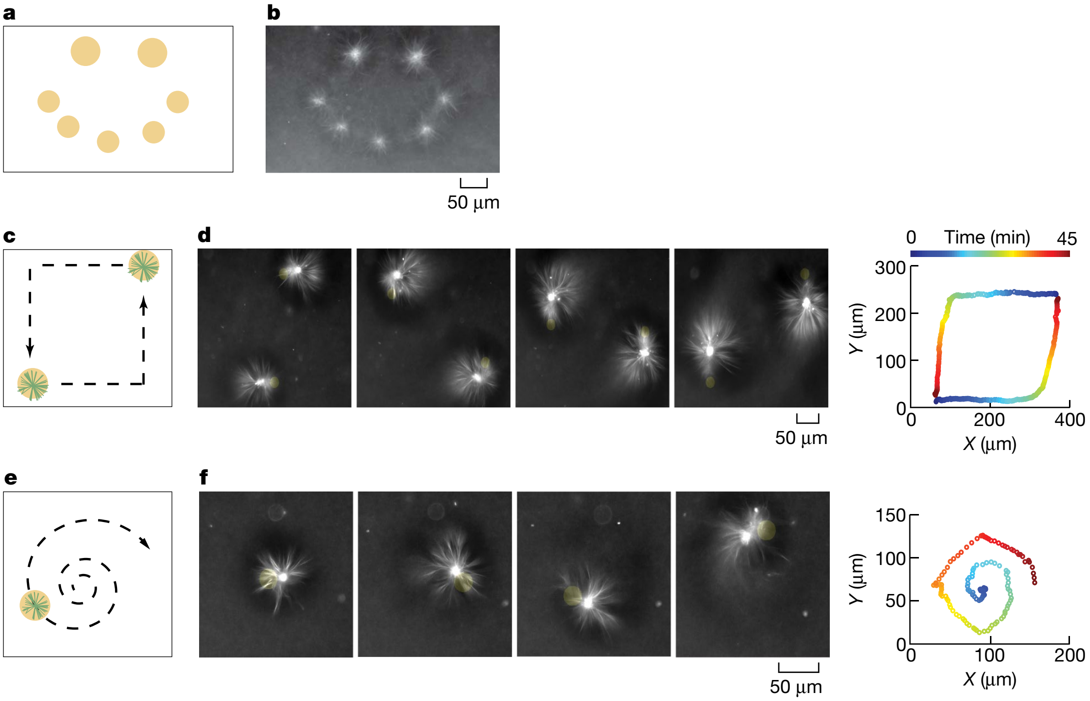

Fig. 3 | Aster creation and moving operations are combined to make different desired patterns and trajectories. a, Use of excitation cylinders to simultaneously pattern asters of different sizes. **b**, Resultant pattern of asters corresponding to **a**. **c**, Illustration of simultaneous control of two different aster trajectories, indicated by the dashed arrows. **d**, Time-lapse images (left) and two-dimensional trace (right) of the aster trajectories in **c**. The trajectory trace is colour-coded to represent progression in time. **e**, Dynamically projected spiral illustrating curvilinear motion. **f**, Time-lapse images (left) and two-dimensional trace (right) of the aster trajectory. Time is colour-coded as in **d**.

of molecular activity. Having the capability to simultaneously generate and manipulate asters provides a basis for 'programming' complex systems of interacting non-equilibrium structures.

In our aster merging, moving and trajectory experiments, we observe fluid flow of the buffer, as inferred by the advection of microtubules and small fluorescent aggregates. Similar cytoskeletal-driven flow is critical for the development and morphogenesis of various unicellular and multicellular organisms[21–27].

On the basis of these observations, we seek to generate and tune flows in our engineered system with light, which may also provide insight into the mechanics of cellular fluid flow. Recent work used light to thermally induce cytoplasmic flows[28]. Here, we can generate fluid flows with light by activating contractile microtubule networks with a rectangular-bar pattern used during aster merging (Fig. 4a, Supplementary Video 9). Bright-field images reveal a structurally changing microtubule network (Fig. 4b, Supplementary Video 10), which appears to drive the fluid flow. We observe that there are minimum size and angle limits for these microtubule structures, as well as for asters (Supplementary Information section 2.17).

We measure the flow fields with tracer particles (Supplementary Information section 2.18). The pattern of the flow is two-dimensional (Supplementary Information section 2.19) and stable throughout the experiment (Supplementary Information section 2.20), consisting of inflows and outflows of microtubules, as illustrated by streamline plots (Fig. 4c, Supplementary Information section 2.21). The competition of these flows ensures that microtubules do not continuously accumulate in the illuminated region and that the surrounding medium is not completely depleted of microtubules.

We manipulate the properties of the flow field through the geometry of the activation volume. The size (Supplementary Information section 2.22) and speed of the flow field depend linearly on the length of the activation bar (Fig. 4d, e). The scaling of the flow speed is similar to the relationships of the formation rate with the activation diameter and of the aster merging speed with the separation. The positioning and number of inflows, outflows and vortices are determined by the extrema of the light pattern geometry (Fig. 4f, g, Supplementary Videos 11–13). A model that uses a series of point forces following the observed microtubule networks is able to recreate similar inflows and outflows (Supplementary Information section 2.23), suggesting that forces from microtubule bundles drive the flow.

Furthermore, the shape of the flow field has a temporal dependence on the light pattern. We modulate the flow field to create an 'active stir bar' by applying a rotating light pattern (Fig. 4h, Supplementary Video 14). Whereas simplified active-matter systems can spontaneously generate global flows[6,8], in vivo cytoskeletal-driven fluid flows can be controlled and highly structured[21,22,26]. Our results demonstrate the creation and dynamic manipulation of localized, structured fluid flow in an engineered active-matter system.

In this work, we uncover active-matter phenomena through the creation and manipulation of non-equilibrium structures and resultant fluid flows. Our ability to define boundaries of protein activity with light enables unprecedented control of the organization of an active-matter system (Supplementary Information section 2.25). We determine the scaling rules of contractile networks and induce movement of non-equilibrium structures and modulation of flow fields. This framework may be built upon to create active-matter devices that control fluid flow. Future work will explore spatiotemporal limits of non-equilibrium structures and the interplay of mass flows and structural changes, and develop new theories of non-equilibrium mechanics and dynamics. Our approach of understanding through construction creates a path towards a generalizable theory of non-equilibrium systems, engineering with active matter and understanding biological phenomena.

Data availability

The data that support the findings of this study are available from the Caltech Research Data Repository at https://data.caltech.edu/records/1160. All plasmids used in this study are available at https://www.addgene.org. All of the other reagents and the source code used for this study are available from the corresponding authors upon reasonable request.

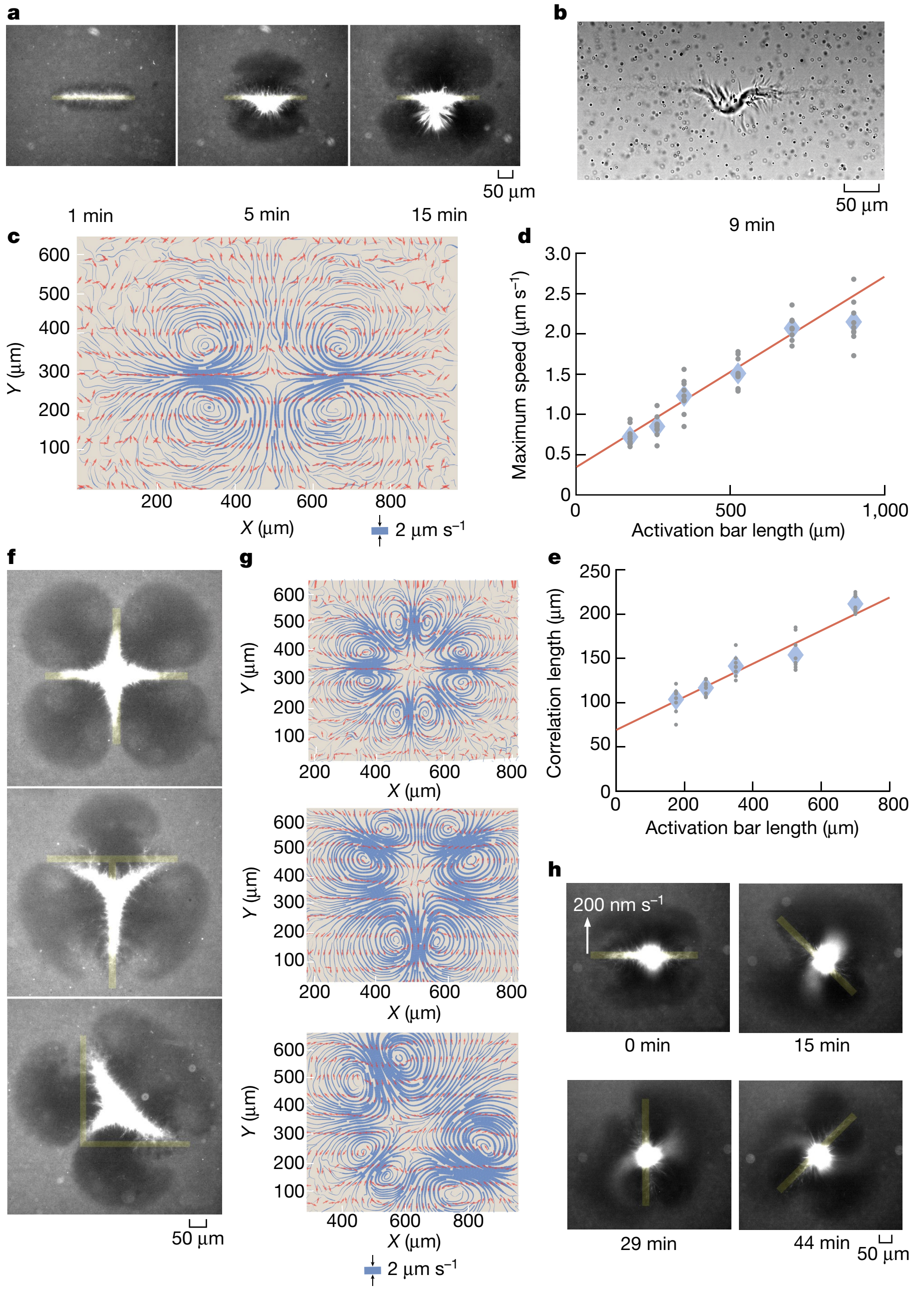

Fig. 4 | Advective fluid flow is created and controlled with patterned light. a, Microtubule organization created by a rectangular 350 µm × 20 µm activation bar. The time-series images demonstrate continuous contraction of microtubules towards the pattern centre along the major axis. **b**, Bright-field image of **a**, showing a contracting microtubule network, as well as the tracer particles that are tracked to measure fluid flow. **c**, Streamline plot of background buffer flow from **a**. The streamline thickness represents the flow speed and the arrows indicate the flow direction. **d**, Average maximum flow speed versus activation bar length. **e**, Average correlation length (size) of flow field versus activation bar length. **f**, **g**, Superposition of activation bars generating different patterns of contractile microtubules (**f**) and corresponding streamline plots (**g**). **h**, Time-lapse images of a light pattern rotating with an edge speed of 200 nm s^{-1}. In **d**, **e** the blue diamonds represents the mean of nine experiments and the grey dots represent individual experiments. The red line is a linear fit to the data. The height of the scale bar in **c**, **g** corresponds to the width of the streamlines.

Online content

Any methods, additional references, Nature Research reporting summaries, source data, extended data, supplementary information, acknowledgements, peer review information; details of author contributions and competing interests; and statements of data and code availability are available at https://doi.org/10.1038/s41586-019-1447-1.

Received: 11 January 2019; Accepted: 5 June 2019;
Published online 7 August 2019.

1. Marchetti, M. C. et al. Hydrodynamics of soft active matter. *Rev. Mod. Phys.* **85**, 1143–1189 (2013).
2. Dumont, S. & Prakash, M. Emergent mechanics of biological structures. *Mol. Biol. Cell* **25**, 3461–3465 (2014).
3. Needleman, D. & Dogic, Z. Active matter at the interface between materials science and cell biology. *Nat. Rev. Mater.* **2**, 17048 (2017).
4. Nédélec, F. J., Surrey, T., Maggs, A. C. & Leibler, S. Self-organization of microtubules and motors. *Nature* **389**, 305–308 (1997).
5. Surrey, T., Nédélec, F., Leibler, S. & Karsenti, E. Physical properties determining self-organization of motors and microtubules. *Science* **292**, 1167–1171 (2001).
6. Sanchez, T., Chen, D. T. N., DeCamp, S. J., Heymann, M. & Dogic, Z. Spontaneous motion in hierarchically assembled active matter. *Nature* **491**, 431–434 (2012).
7. DeCamp, S. J., Redner, G. S., Baskaran, A., Hagan, M. F. & Dogic, Z. Orientational order of motile defects in active nematics. *Nat. Mater.* **14**, 1110 (2015).
8. Wu, K.-T. et al. Transition from turbulent to coherent flows in confined three-dimensional active fluids. *Science* **355**, eaal1979 (2017).

9. Bricard, A., Caussin, J.-B., Desreumaux, N., Dauchot, O. & Bartolo, D. Emergence of macroscopic directed motion in populations of motile colloids. *Nature* **503**, 95–98 (2013).
10. Nédélec, F., Surrey, T. & Maggs, A. C. Dynamic concentration of motors in microtubule arrays. *Phys. Rev. Lett.* **86**, 3192–3195 (2001).
11. Lee, H. Y. & Kardar, M. Macroscopic equations for pattern formation in mixtures of microtubules and molecular motors. *Phys. Rev. E* **64**, 056113 (2001).
12. Keber, F. C. et al. Topology and dynamics of active nematic vesicles. *Science* **345**, 1135–1139 (2014).
13. Aoyama, S., Shimoike, M. & Hiratsuka, Y. Self-organized optical device driven by motor proteins. *Proc. Natl Acad. Sci. USA* **110**, 16408–16413 (2013).
14. Guntas, G. et al. Engineering an improved light-induced dimer (iLID) for controlling the localization and activity of signaling proteins. *Proc. Natl Acad. Sci. USA* **112**, 112–117 (2015).
15. Schuppler, M., Keber, F. C., Kröger, M. & Bausch, A. R. Boundaries steer the contraction of active gels. *Nat. Commun*. **7**, 13120 (2016).
16. Belmonte, J. M., Leptin, M. & Nédélec, F. A theory that predicts behaviors of disordered cytoskeletal networks. *Mol. Syst. Biol*. **13**, 941 (2017).
17. Foster, P. J., Fürthauer, S., Shelley, M. J. & Needleman, D. J. Active contraction of microtubule networks. *eLife* **4**, e10837 (2015).
18. Good, M. C., Vahey, M. D., Skandarajah, A., Fletcher, D. A. & Heald, R. Cytoplasmic volume modulates spindle size during embryogenesis. *Science* **342**, 856–860 (2013).
19. Weiner, O. D., Marganski, W. A., Wu, L. F., Altschuler, S. J. & Kirschner, M. W. An actin-based wave generator organizes cell motility. *PLoS Biol*. **5**, e221 (2007).
20. Gardel, M. L., Schneider, I. C., Aratyn-Schaus, Y. & Waterman, C. M. Mechanical integration of actin and adhesion dynamics in cell migration. *Annu. Rev. Cell Dev. Biol*. **26**, 315–333 (2010).
21. Theurkauf, W. E. Premature microtubule-dependent cytoplasmic streaming in cappuccino and spire mutant oocytes. *Science* **265**, 2093–2096 (1994).
22. Ganguly, S., Williams, L. S., Palacios, I. M. & Goldstein, R. E. Cytoplasmic streaming in *Drosophila* oocytes varies with kinesin activity and correlates with the microtubule cytoskeleton architecture. *Proc. Natl Acad. Sci. USA* **109**, 15109–15114 (2012).
23. Goldstein, R. E., Tuval, I. & van de Meent, J.-W. Microfluidics of cytoplasmic streaming and its implications for intracellular transport. *Proc. Natl Acad. Sci. USA* **105**, 3663–3667 (2008).
24. Drescher, K., Dunkel, J., Cisneros, L. H., Ganguly, S. & Goldstein, R. E. Fluid dynamics and noise in bacterial cell–cell and cell–surface scattering. *Proc. Natl Acad. Sci. USA* **108**, 10940–10945 (2011).
25. Drescher, K., Goldstein, R. E., Michel, N., Polin, M. & Tuval, I. Direct measurement of the flow field around swimming microorganisms. *Phys. Rev. Lett.* **105**, 168101 (2010).
26. He, B., Doubrovinski, K., Polyakov, O. & Wieschaus, E. Apical constriction drives tissue-scale hydrodynamic flow to mediate cell elongation. *Nature* **508**, 392–396 (2014).
27. Shinar, T., Mana, M., Piano, F. & Shelley, M. J. A model of cytoplasmically driven microtubulebased motion in the single-celled *Caenorhabditis elegans* embryo. *Proc. Natl Acad. Sci. USA* **108**, 10508–10513 (2011).
28. Mittasch, M. et al. Non-invasive perturbations of intracellular flow reveal physical principles of cell organization. *Nat. Cell Biol*. **20**, 344–351 (2018).

Publisher’s note: Springer Nature remains neutral with regard to jurisdictional claims in published maps and institutional affiliations.

© The Author(s), under exclusive licence to Springer Nature Limited 2019

Acknowledgements We thank M. Anjur-Dietrich, J. Brady, J. Bruck, V. Galstyan, S. Hirokawa, C. Hueschen, Y. Lazebnik, W. Lim, W. Marshall, D. Mullins, D. Needleman, P. Rothemund and E. Winfree for scientific discussions. We thank L. Bugaj, Z. Dogic, A. Frost, W. Huynh, R. Ismagilov, L. Metcalf, H. Nguyen and R. Vale for advice and assistance during the development of the experimental system; K. van den Dries for assistance with three-dimensional visualization of asters; P. Sternberg for use of a microscopy system for initial light-activation experiments. We are grateful to N. Orme for assistance with figures and illustrations. We acknowledge support from the NIH through grants 1R35 GM118043-01 (R.P.) and NIH DP5 OD012194 (M.T.); the NSF through NSF 1330864 (M.T.); the John Templeton Foundation as part of the Boundaries of Life Initiative through grants 51250 & 60973 (R.P.); the Foundational Questions Institute and Fetzer Franklin Fund through FQXi 1816 (R.P., M.T.); and the UCSF Center for Systems and Synthetic Biology NIGMS P50 GM081879 (M.T.). M.T. acknowledges support from the Heritage Medical Research Institute.

Author contributions T.D.R., H.J.L., R.P. and M.T. conceived the experiments and interpreted the results. T.D.R., H.J.L., R.A.B., Z.Q. and M.T. wrote the manuscript. T.D.R. designed and cloned iLID motor fusion constructs. T.D.R., H.J.L. and R.A.B. performed protein purification. T.D.R. and H.J.L. designed, performed and analysed the active-matter experiments. Z.Q. analysed and modelled flow data and tracked trajectories of moving asters. R.A.B. performed and analysed gliding assays. All authors discussed the results and commented on the manuscript.

Competing interests The authors declare no competing interests.

Additional information

Supplementary information is available for this paper at https://doi.org/10.1038/s41586-019-1447-1.

Correspondence and requests for materials should be addressed to T.D.R. or M.T.

Peer review information *Nature* thanks Andreas Bausch, François Nédélec and Suraj Shankar for their contribution to the peer review of this work.

Reprints and permissions information is available at http://www.nature.com/reprints.